Measurements and Structure of the Exosphere

Edwin Mierkiewicz
Embry-Riddle Aeronautical University

S.M. Nossal, F.L. Roesler, D. Gardner
University of Wisconsin Madison

This work is supported by NSF CAREER award: AGS-1352311

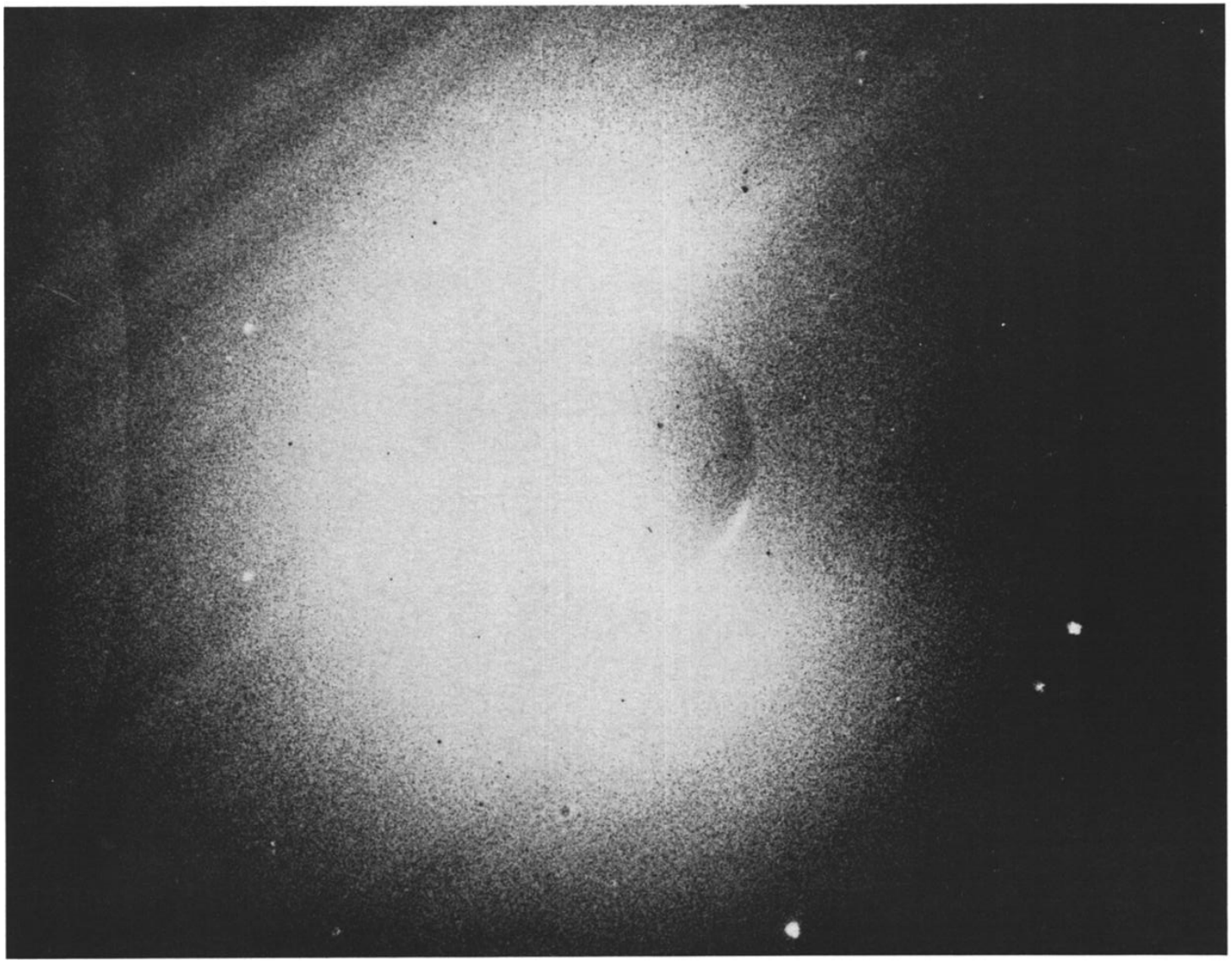

Fig. 1. Print from S-201 frame 40, a 1-min exposure centered on the earth, wavelength range 1050–1600 Å. The hydrogen geocoronal Lyman α emission is the dominant feature. The dark limb is seen silhouetted against the interplanetary Lyman α background. The diagonal streaks in the upper portion of the picture are instrumental.

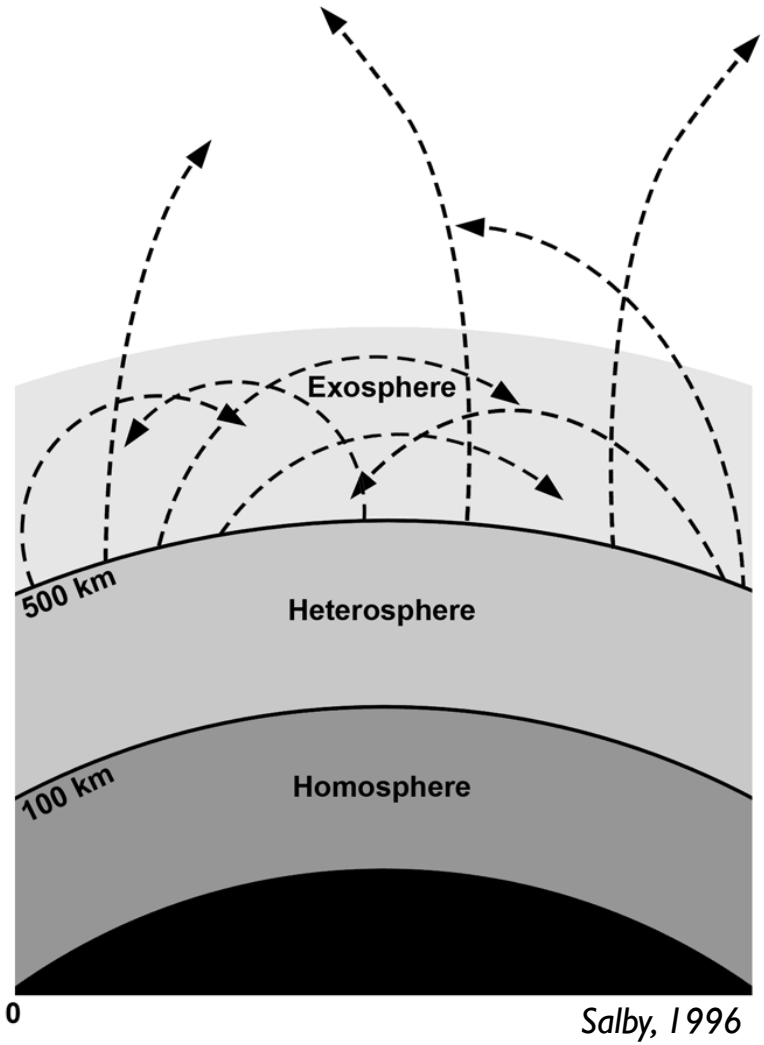

Chemistry
Topside Ionosphere & TEC
Exospheric Physics
Escape
Planetary Evolution/Change
Comparative Aeronomy

Diffusion, ballistic trajectories, photoionization, charge exchange, radiation pressure, and escape to space… all of these things impact the global hydrogen budget…

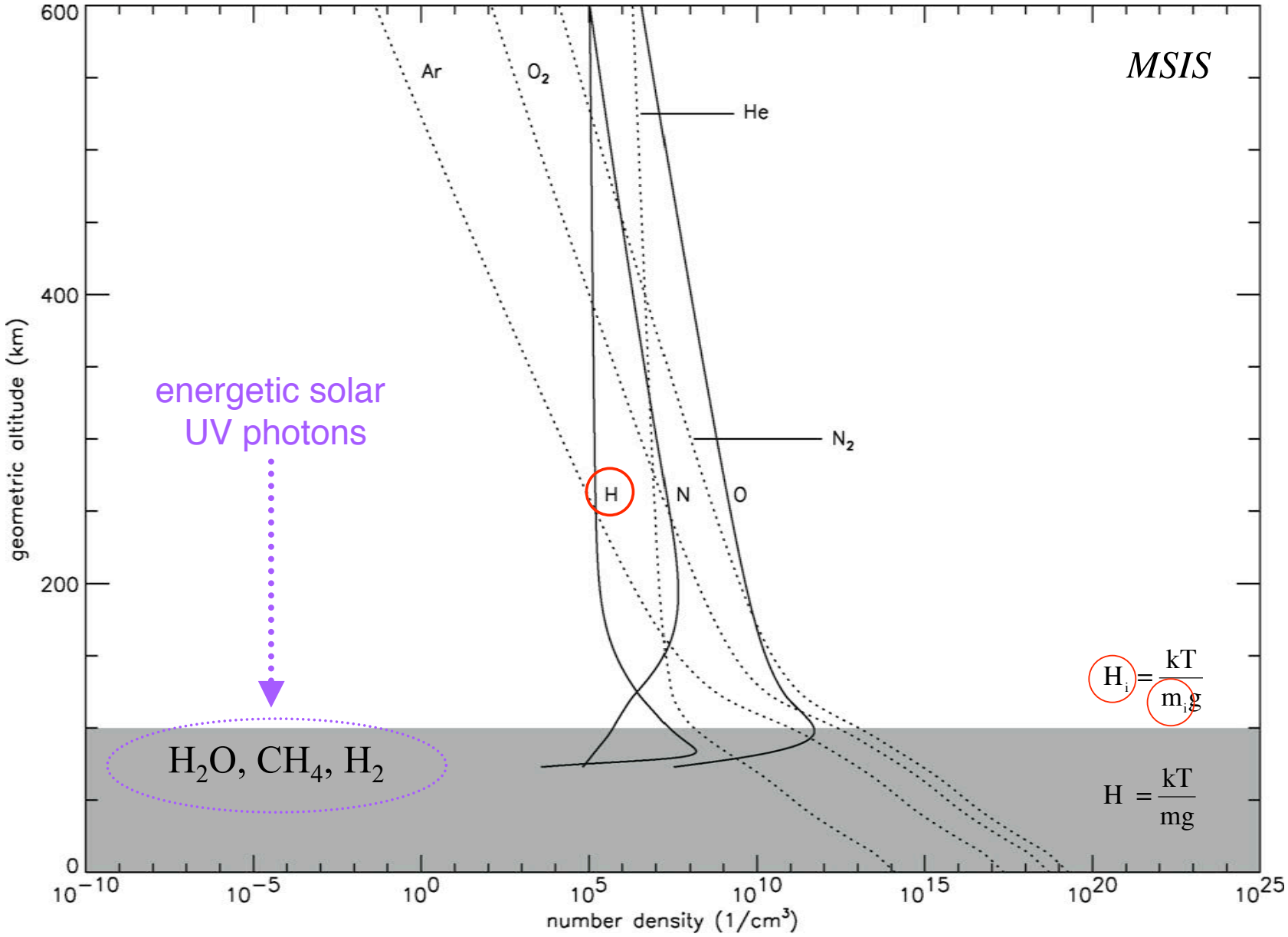
MSIS
Ar
O_2
He
N_2
H
N
O
energetic solar
UV photons
H_2O, CH_4, H_2
$H_i = \frac{kT}{m_i g}$
$H = \frac{kT}{mg}$
geometric altitude (km)
600
400
200
0
10^{-10}
10^{-5}
10^{0}
10^{5}
10^{10}
10^{15}
10^{20}
10^{25}
number density ($1/cm^3$)

the wisconsin H-alpha mapper

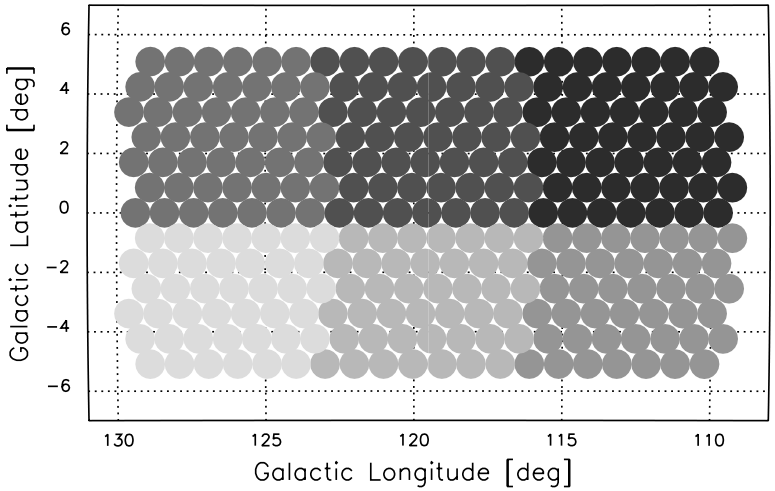
Galactic Latitude [deg]
6
4
2
0
−2
−4
−6
130
125
120
115
110
Galactic Longitude [deg]

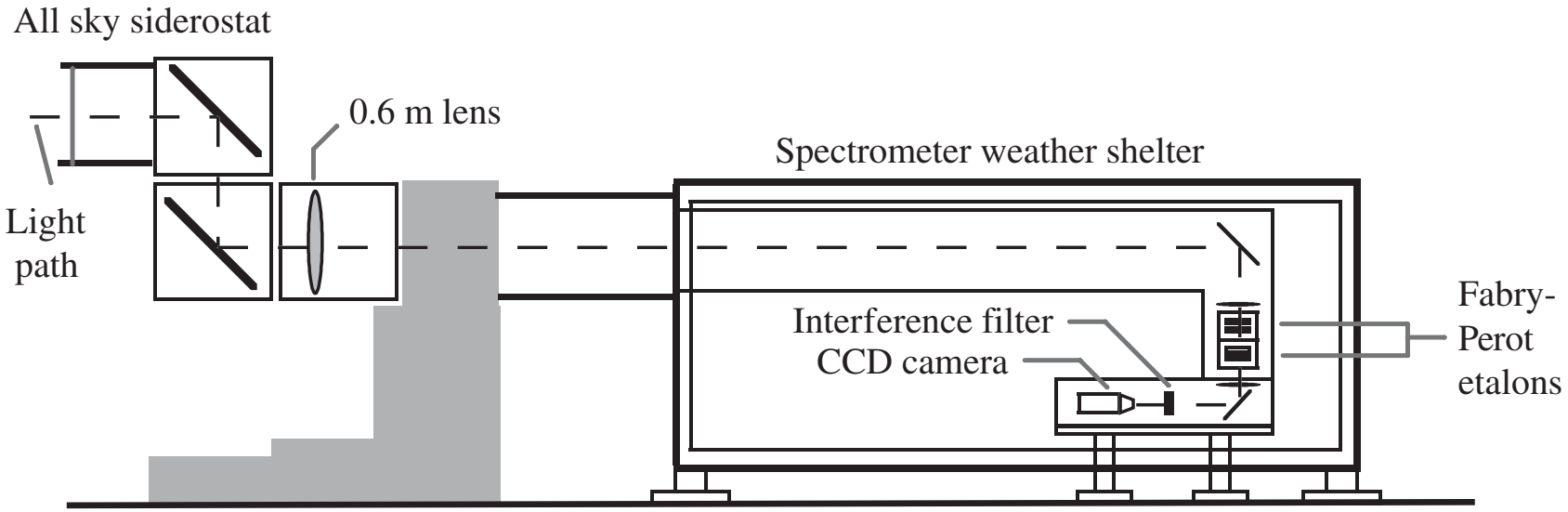
All sky siderostat
0.6 m lens
Spectrometer weather shelter
Light path
Interference filter
CCD camera
Fabry-Perot etalons

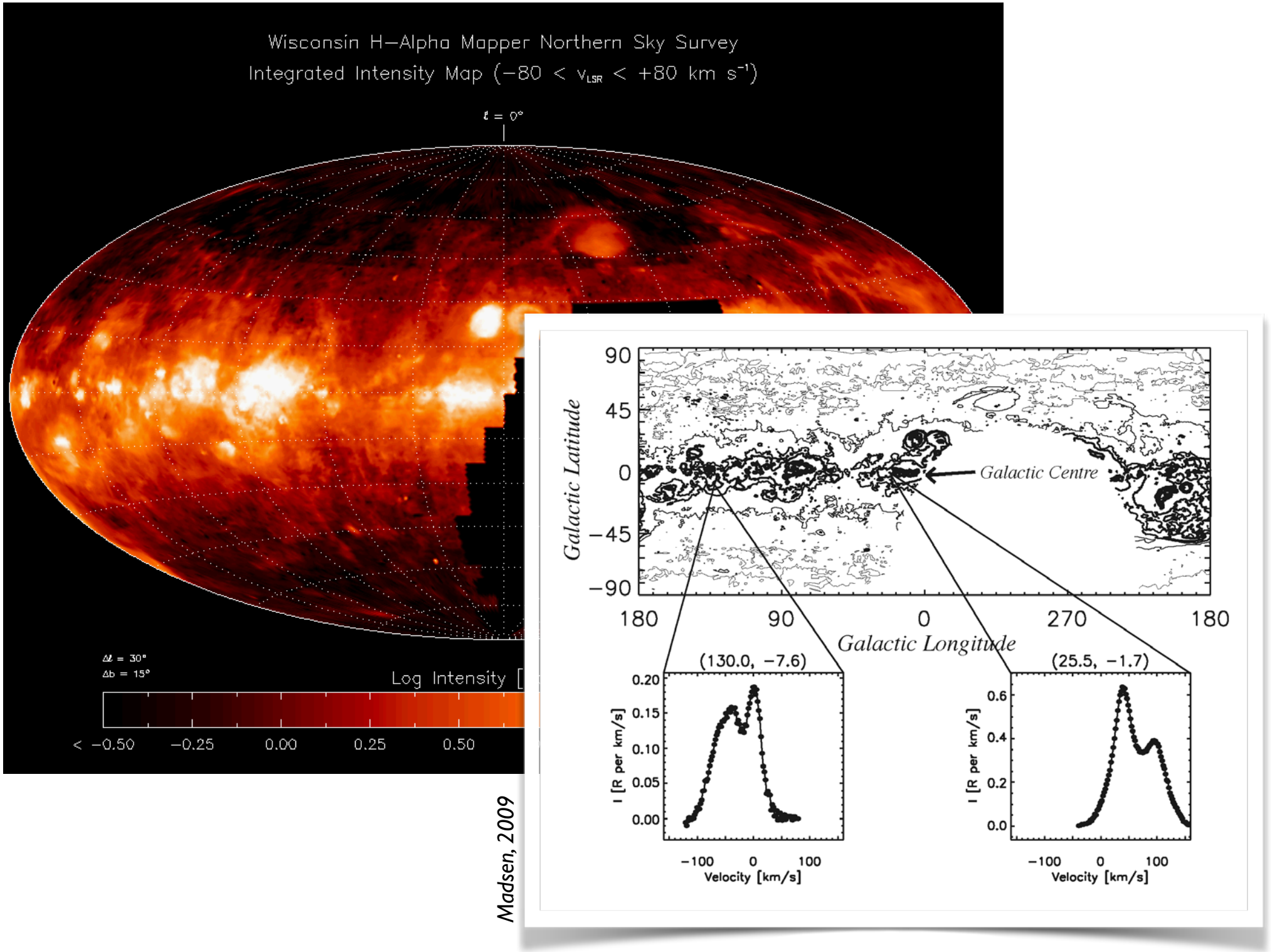
Wisconsin H–Alpha Mapper Northern Sky Survey
Integrated Intensity Map (−80 < v_{LSR} < +80 km s^{-1})
ℓ = 0°
Δℓ = 30°
Δb = 15°
Log Intensity [
< −0.50
−0.25
0.00
0.25
0.50
90
45
0
−45
−90
Galactic Latitude
Galactic Centre
180
90
0
270
180
Galactic Longitude
(130.0, −7.6)
(25.5, −1.7)
I [R per km/s]
0.20
0.15
0.10
0.05
0.00
0.6
0.4
0.2
0.0
−100
0
100
Velocity [km/s]

Madsen, 2009

shadow altitude

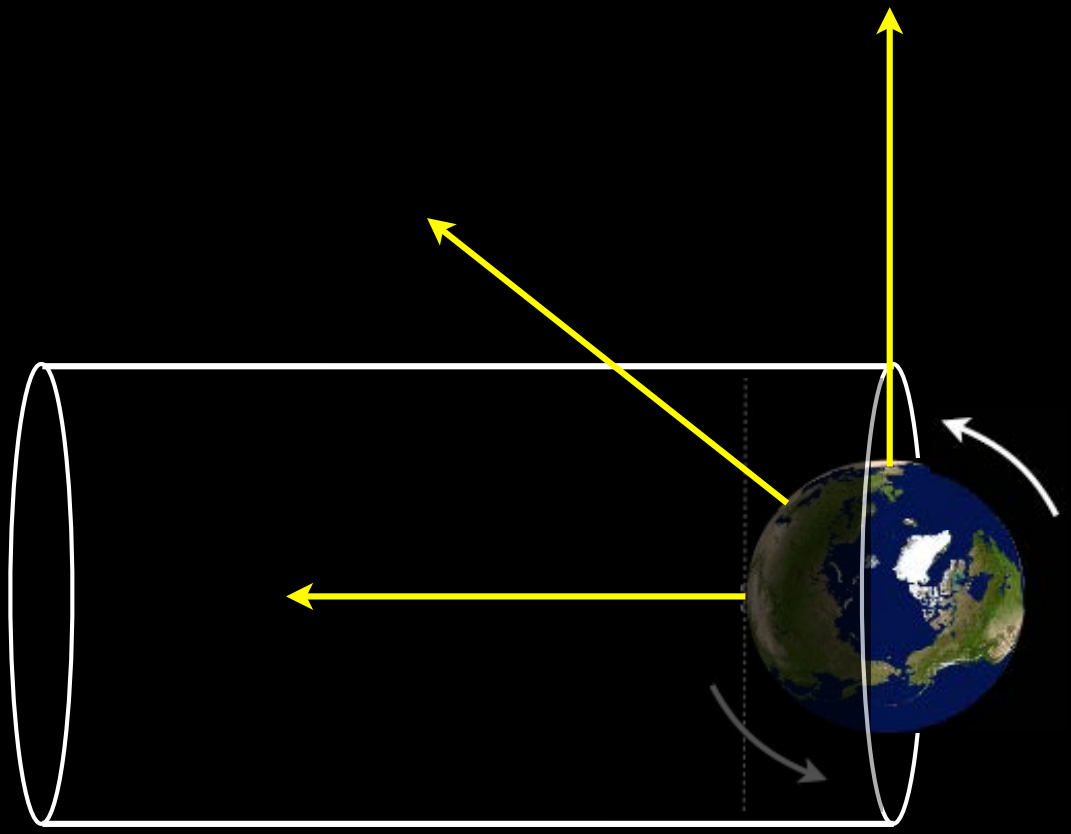

Balmer-alpha and Balmer-beta

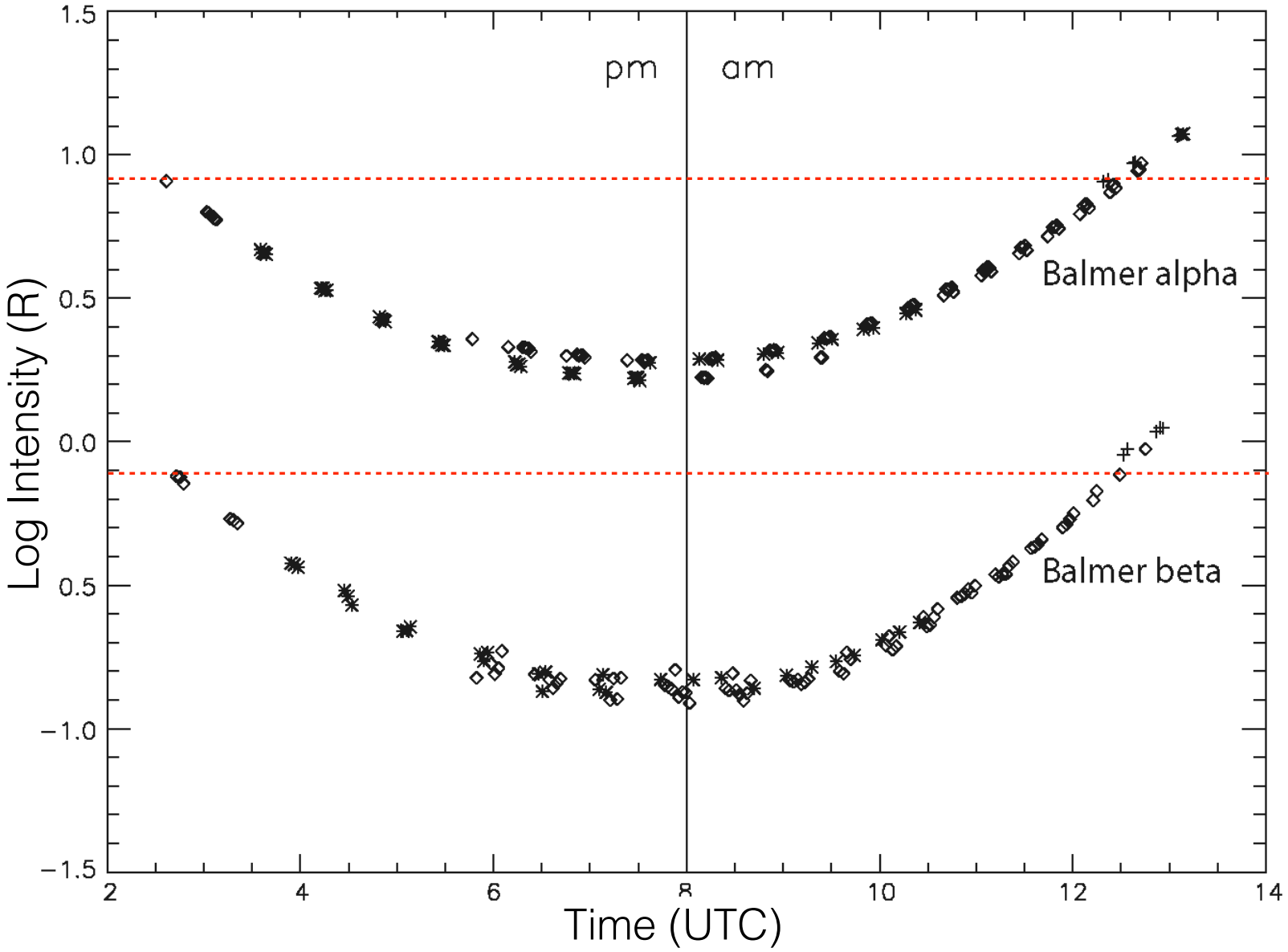

major areas of scientific focus — a ground-based perspective

(1) high resolution observations of the geocoronal hydrogen emission line profile and its relation to excitation mechanisms, effective temperature, and exospheric physics (e.g., Gardner et al., 2016; Mierkiewicz et al., 2012; Nossal et al., 1998, 1997; Kerr & Hecht, 1996; Kerr et al., 1986; Yelle & Roesler, 1985; Meriwether et al., 1980; Atreya et al., 1975)

(2) retrieval of geocoronal hydrogen parameters such as the hydrogen column abundance [H], the hydrogen density profile H(z), and the photochemically initiated hydrogen flux ϕ(H) (e.g., Bishop et al., 2004; He et al., 1993; Kerr & Tepley, 1988)

(3) long term observations of the geocoronal hydrogen column emission intensity for the investigation of natural variability, such as diurnal and solar cycle trends, and possible longer term secular changes (e.g., Nossal et al., 2008; Kerr et al., 2001)

retrieval of geophysical parameters

(1) high resolution observations of the geocoronal hydrogen emission line profile and its relation to excitation mechanisms, effective temperature, and exospheric physics (e.g., Gardner et al., 2016; Mierkiewicz et al., 2012; Nossal et al., 1998, 1997; Kerr & Hecht, 1996; Kerr et al., 1986; Yelle & Roesler, 1985; Meriwether et al., 1980; Atreya et al., 1975)

(2) retrieval of geocoronal hydrogen parameters such as the hydrogen column abundance [H], the hydrogen density profile H(z), and the photochemically initiated hydrogen flux ϕ(H) (e.g., Bishop et al., 2004; He et al., 1993; Kerr & Tepley, 1988)

(3) long term observations of the geocoronal hydrogen column emission intensity for the investigation of natural variability, such as diurnal and solar cycle trends, and possible longer term secular changes (e.g., Nossal et al., 2008; Kerr et al., 2001)

retrieval of geophysical parameters

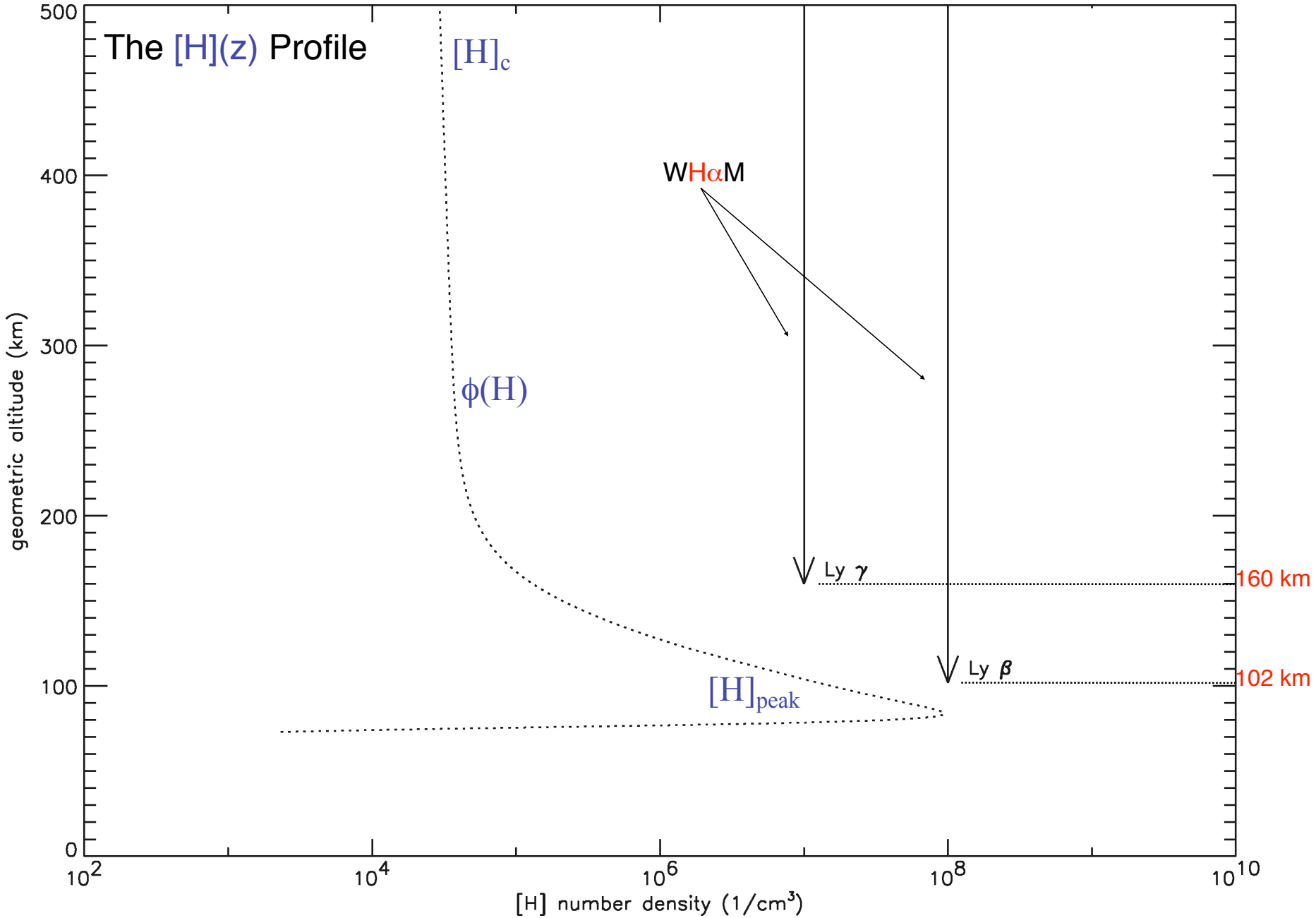

retrieval of geophysical parameters

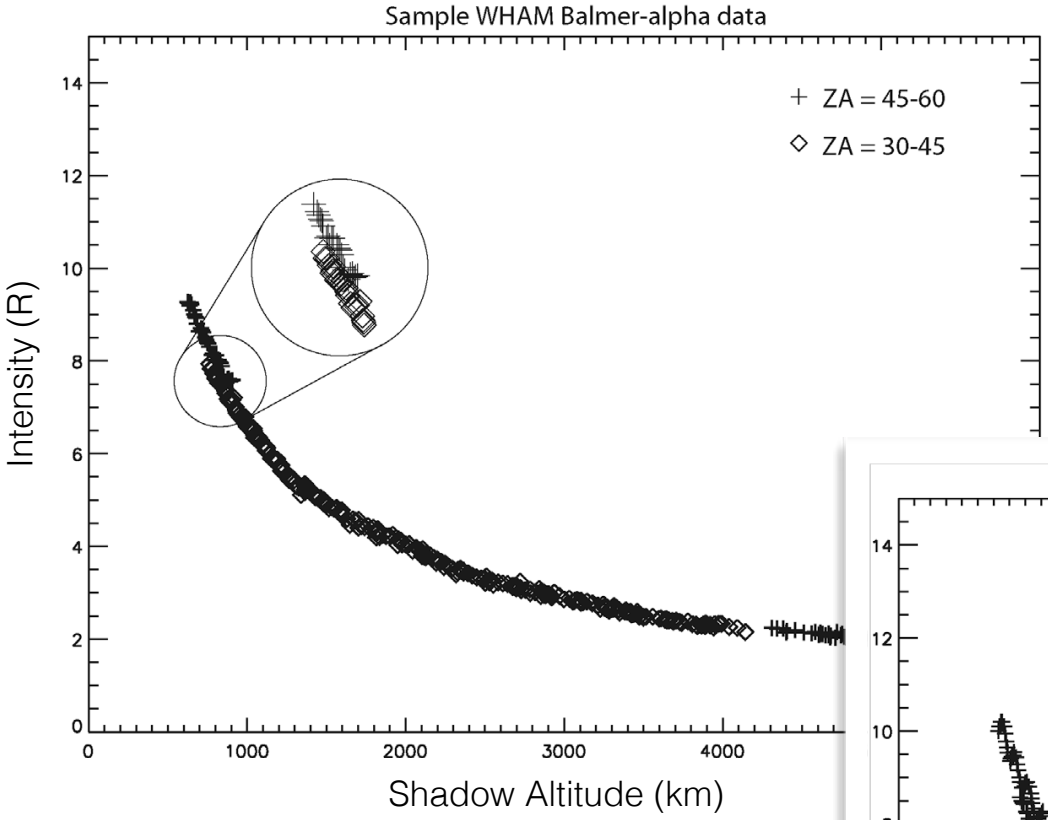

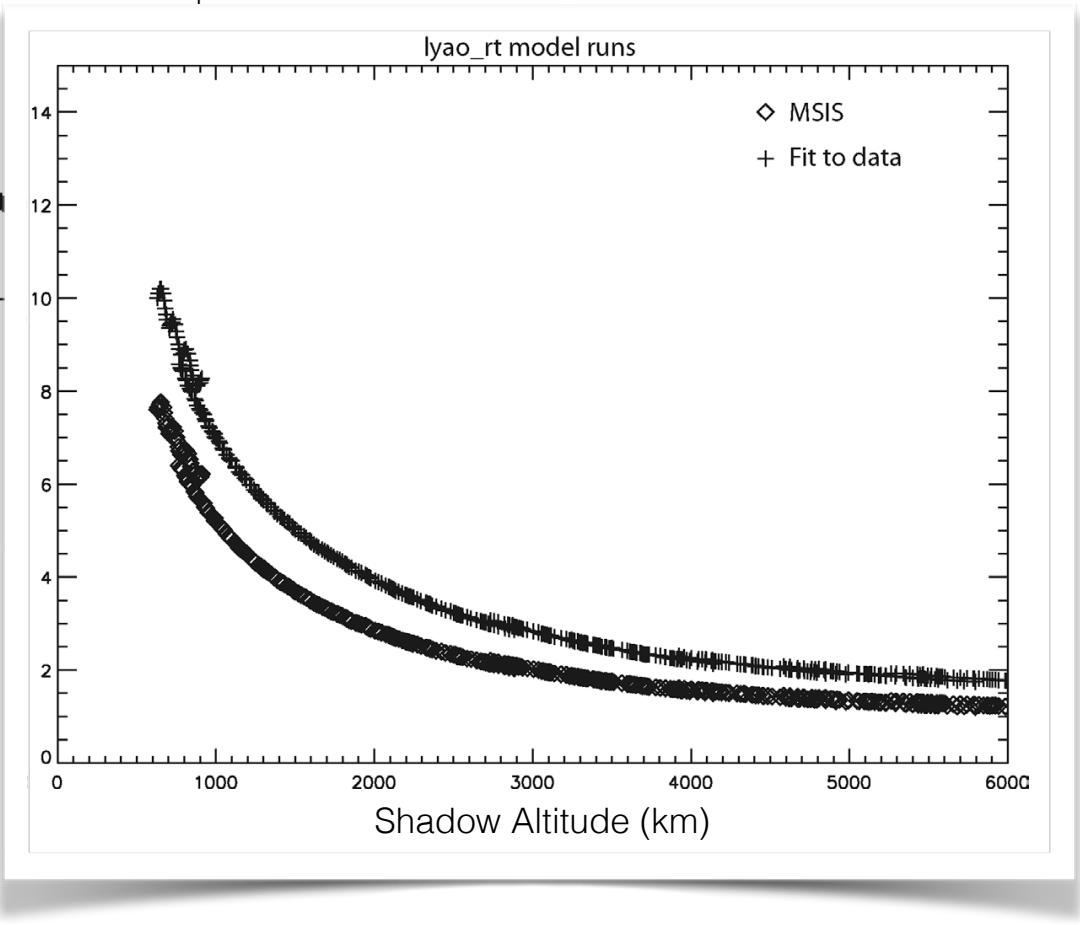

retrieval of geophysical parameters

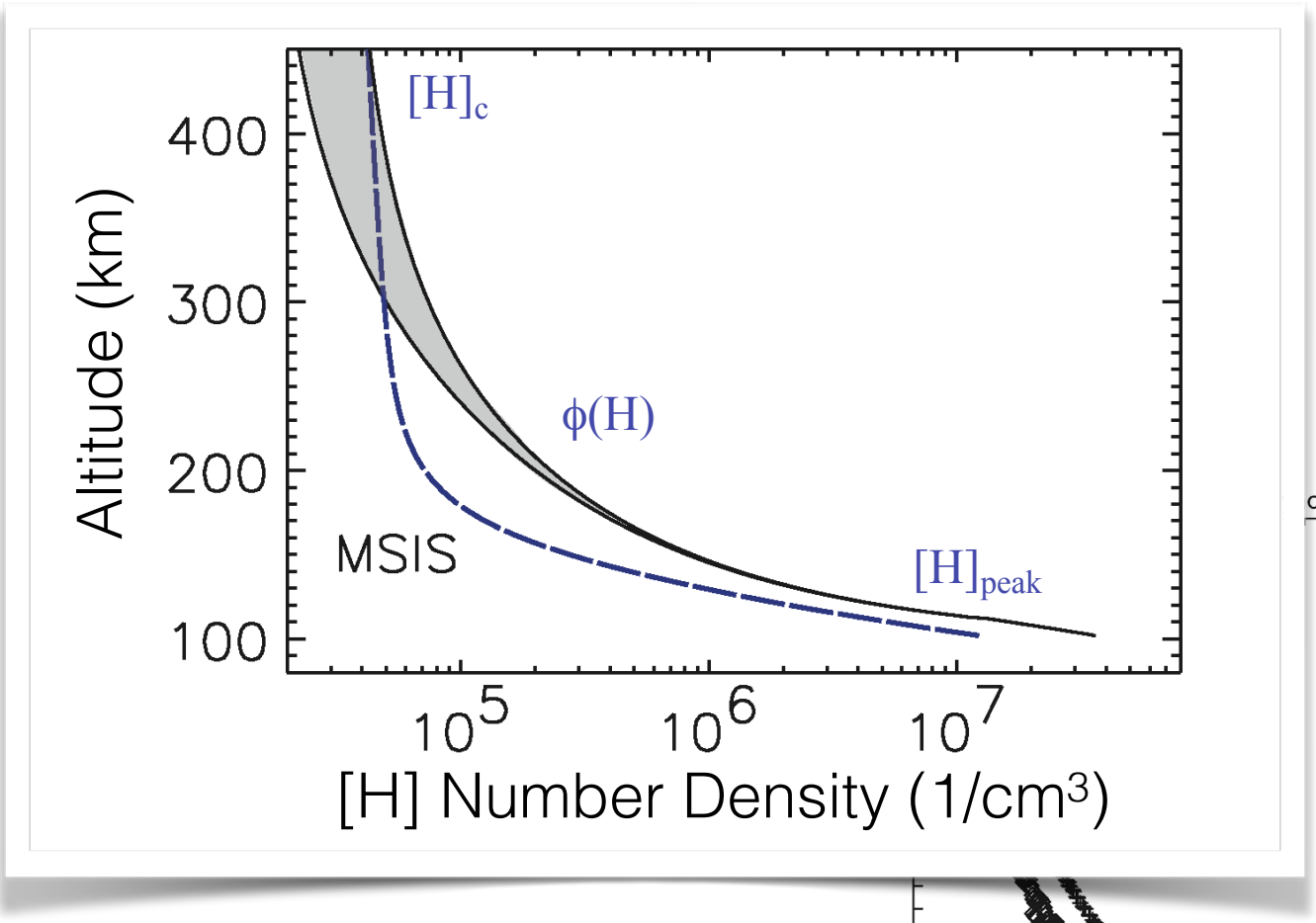

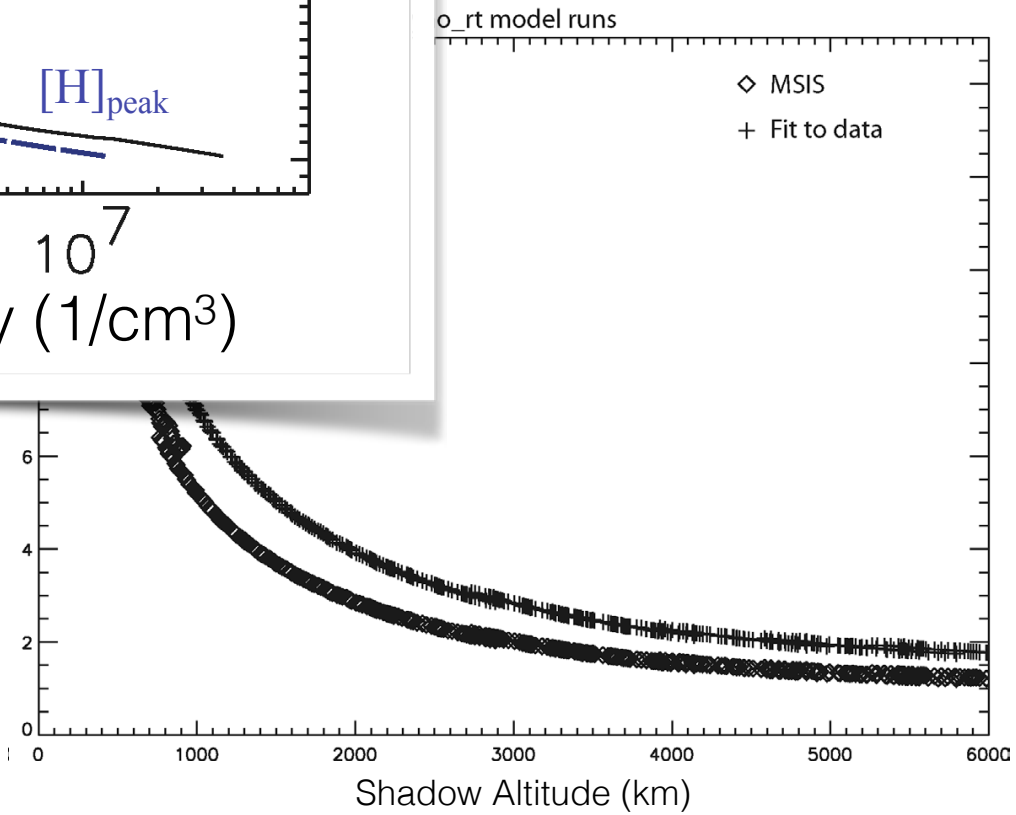

(1) high resolution observations of the geocoronal hydrogen emission line profile and its relation to excitation mechanisms, effective temperature, and exospheric physics (e.g., Gardner et al., 2016; Mierkiewicz et al., 2012; Nossal et al., 1998, 1997; Kerr & Hecht, 1996; Kerr et al., 1986; Yelle & Roesler, 1985; Meriwether et al., 1980; Atreya et al., 1975)

(2) retrieval of geocoronal hydrogen parameters such as the hydrogen column abundance [H], the hydrogen density profile H(z), and the photochemically initiated hydrogen flux ϕ(H) (e.g., Bishop et al., 2004; He et al., 1993; Kerr & Tepley, 1988)

(3) long term observations of the geocoronal hydrogen column emission intensity for the investigation of natural variability, such as diurnal and solar cycle trends, and possible longer term secular changes (e.g., Nossal et al., 2008; Kerr et al., 2001)

line profiles

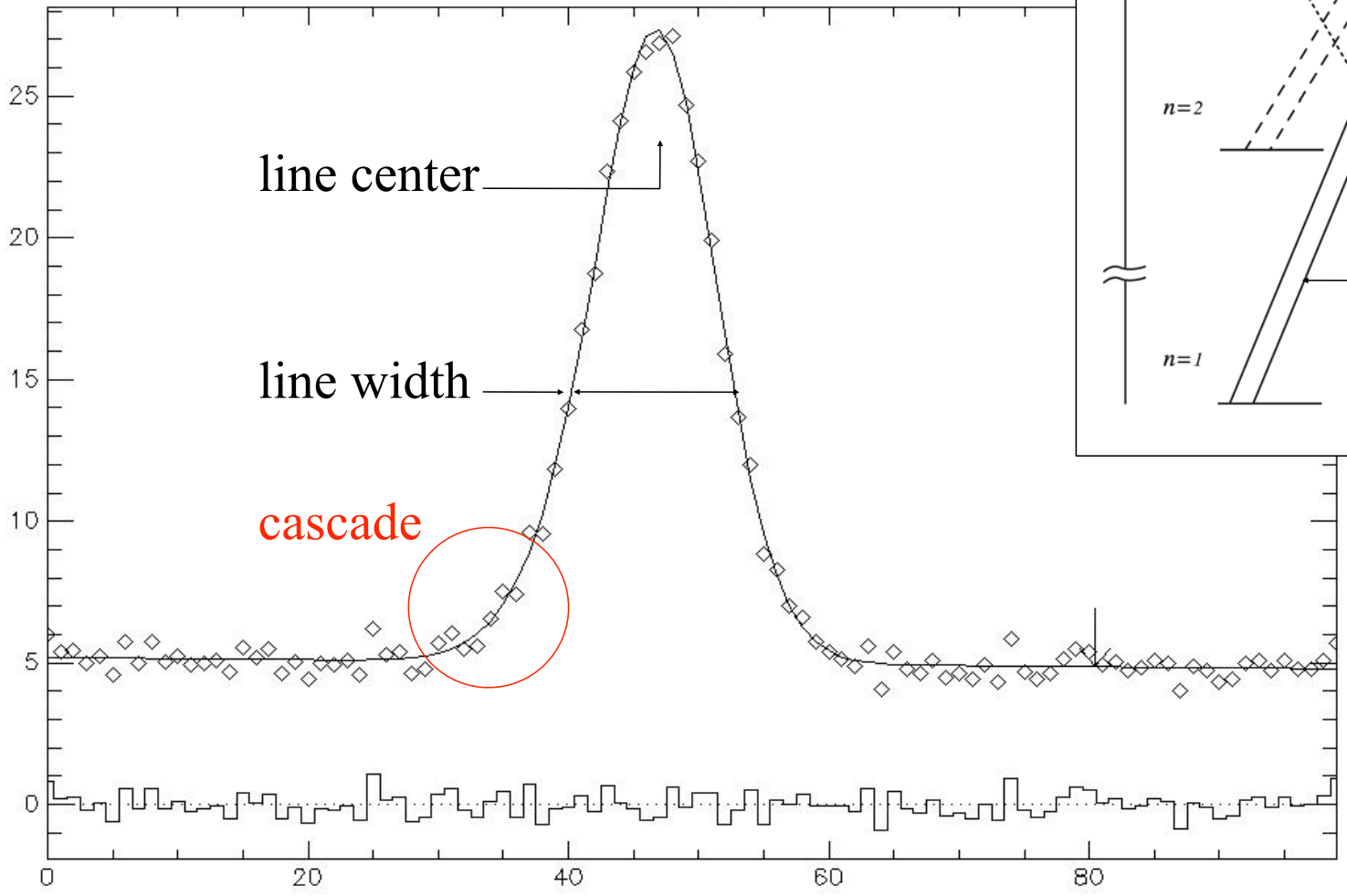

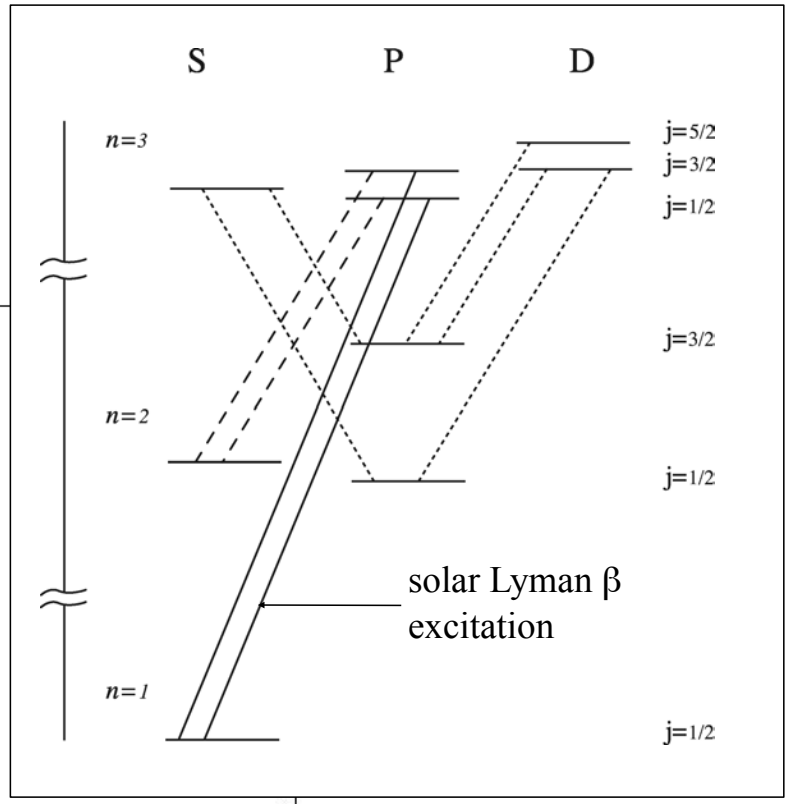

effective temperature

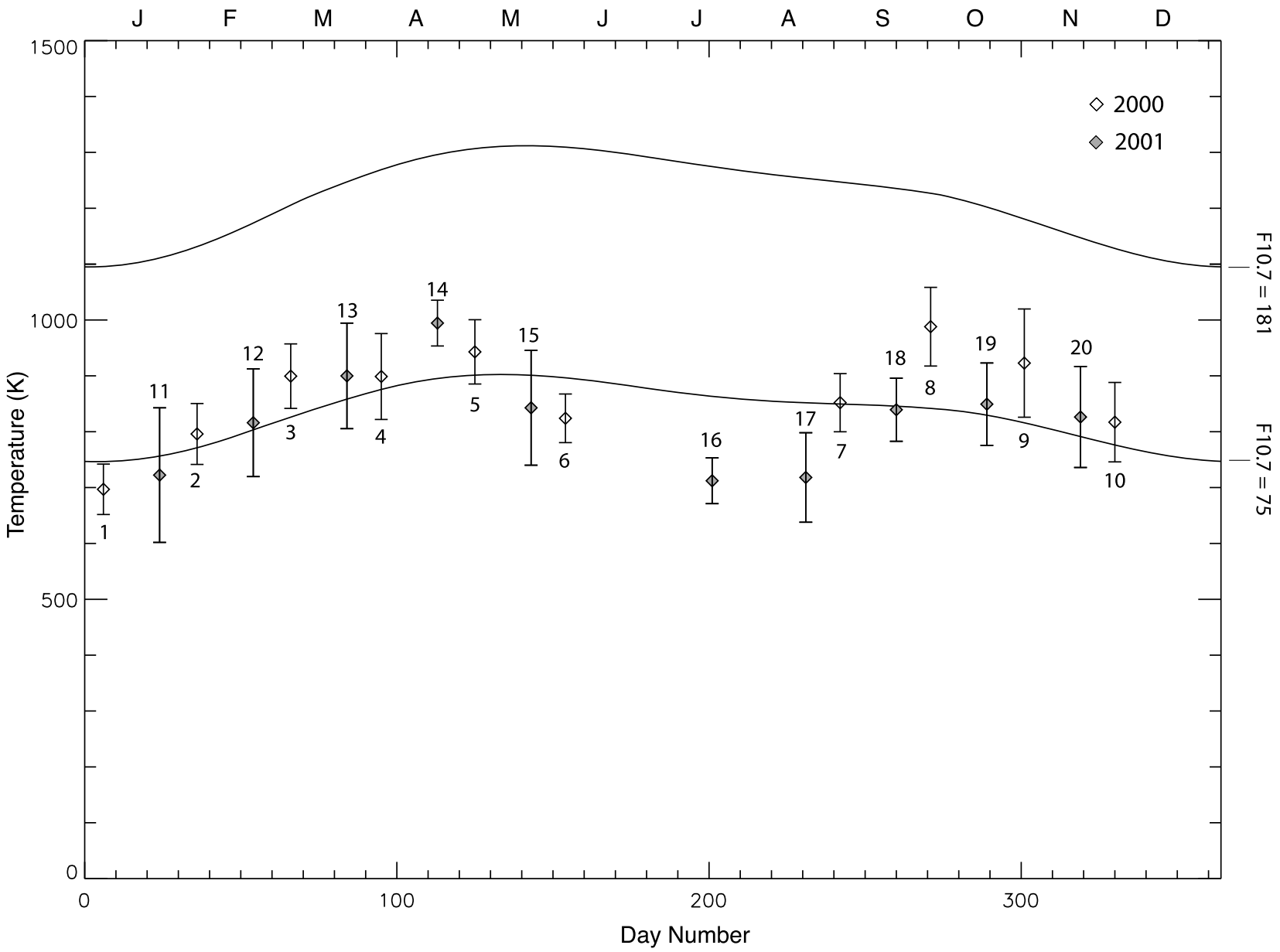

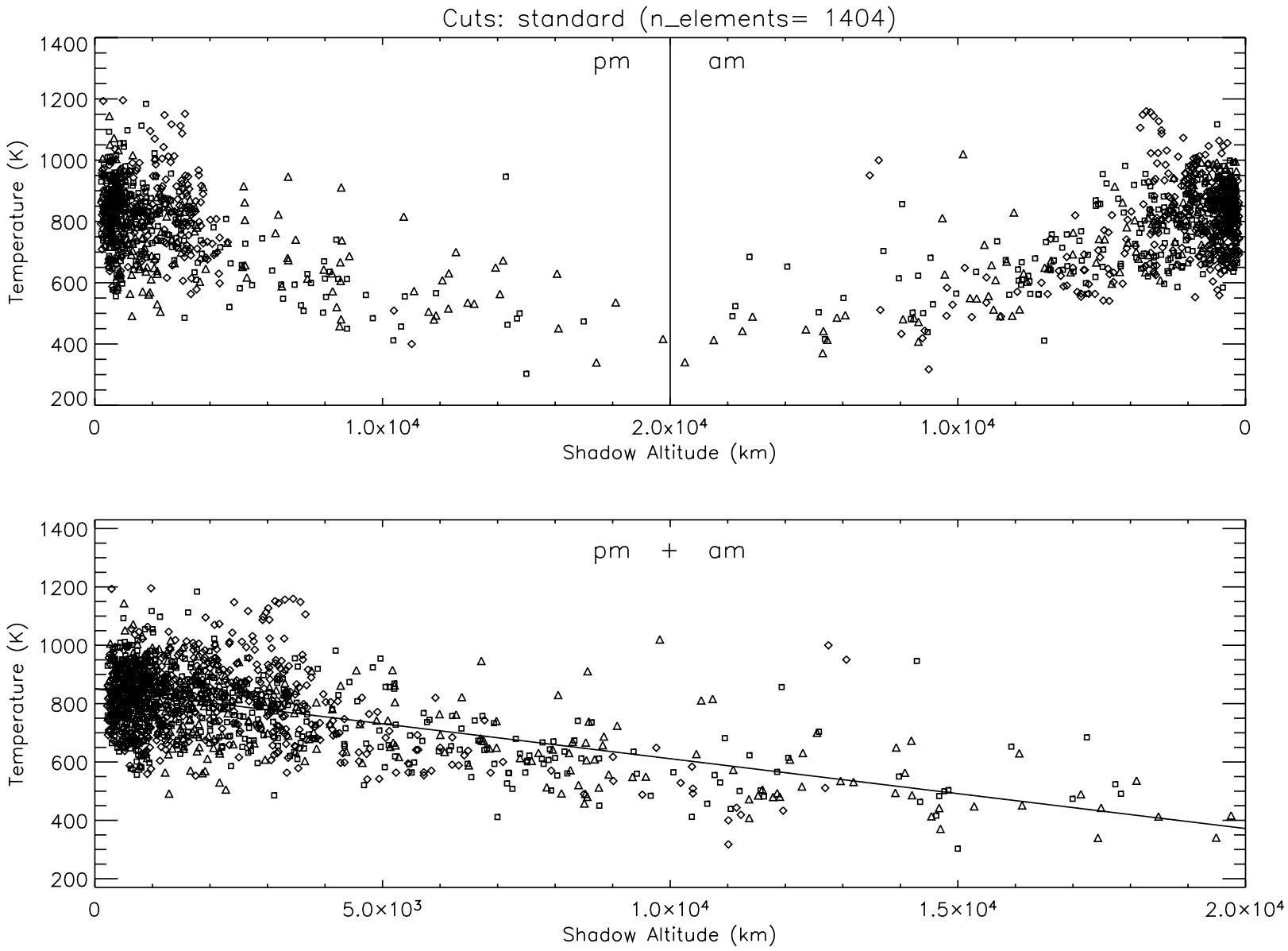
Cuts: standard (n_elements= 1404)
pm
am
Temperature (K)
1400
1200
1000
800
600
400
200
0
1.0x10⁴
2.0x10⁴
1.0x10⁴
0
Shadow Altitude (km)
pm + am
Temperature (K)
1400
1200
1000
800
600
400
200
0
5.0x10³
1.0x10⁴
1.5x10⁴
2.0x10⁴
Shadow Altitude (km)

natural variability

(1) high resolution observations of the geocoronal hydrogen emission line profile and its relation to excitation mechanisms, effective temperature, and exospheric physics (e.g., Gardner et al., 2016; Mierkiewicz et al., 2012; Nossal et al., 1998, 1997; Kerr & Hecht, 1996; Kerr et al., 1986; Yelle & Roesler, 1985; Meriwether et al., 1980; Atreya et al., 1975)

(2) retrieval of geocoronal hydrogen parameters such as the hydrogen column abundance [H], the hydrogen density profile H(z), and the photochemically initiated hydrogen flux ϕ(H) (e.g., Bishop et al., 2004; He et al., 1993; Kerr & Tepley, 1988)

(3) long term observations of the geocoronal hydrogen column emission intensity for the investigation of natural variability, such as diurnal and solar cycle trends, and possible longer term secular changes (e.g., Nossal et al., 2008; Kerr et al., 2001)

natural variability

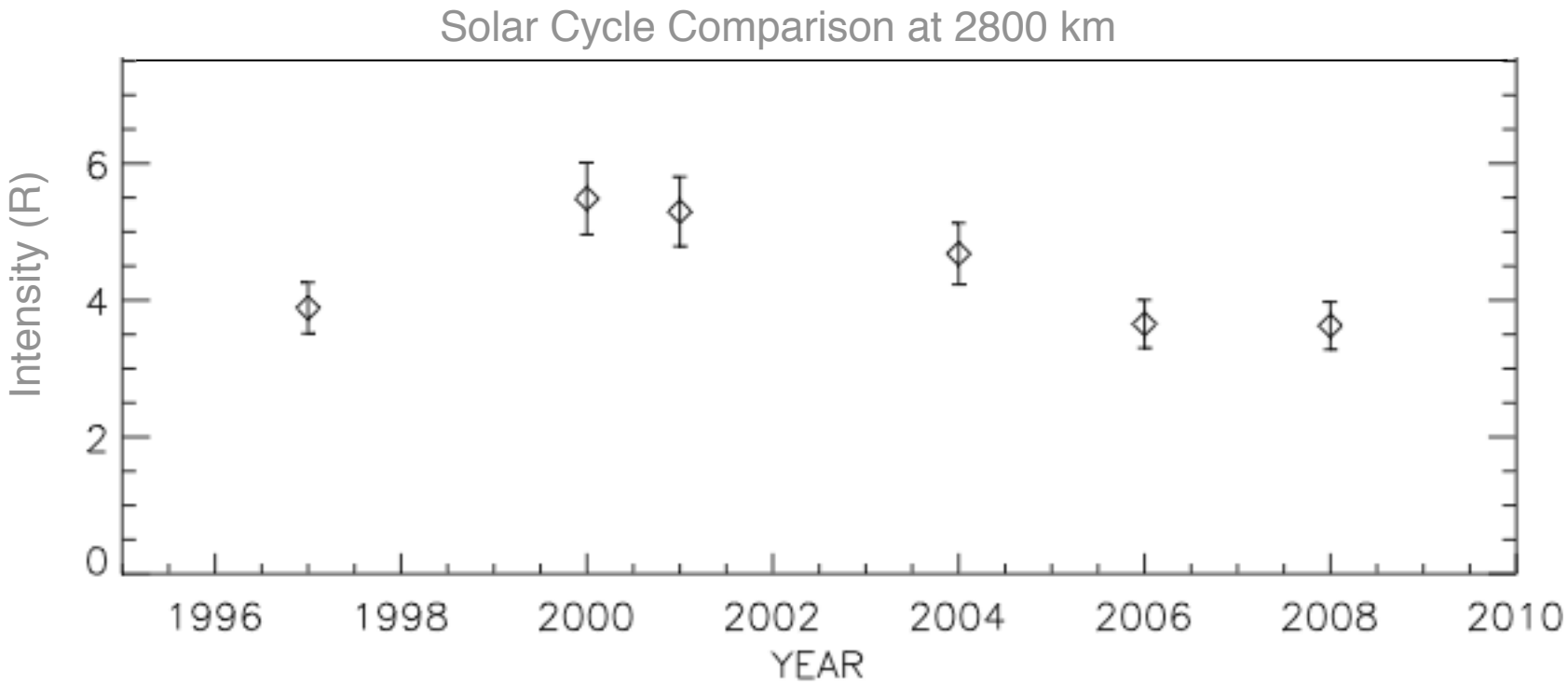

EXOCUBE and ExoDyn, with mass specs capable of measuring atomic mass 1!

GOLD - Exobase Temperatures

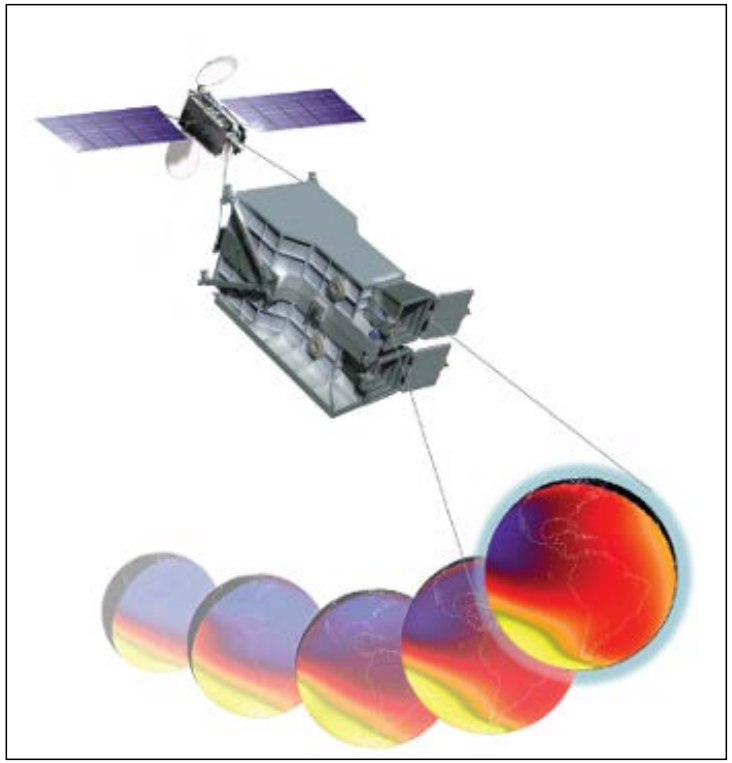

TIMED/GUVI - Lyman-alpha

European SpaceCraft for the study of Atmospheric Particle Escape (ESCAPE)

Core team members:

I. Dandouras <Iannis.Dandouras@irap.omp.eu> (**Lead proposer:** single-point of contact)
CNRS and Paul Sabatier Toulouse University, Institut de Recherche en Astrophysique et Planétologie (IRAP), 9 avenue du Colonel Roche, BP 44346, F-31028 Toulouse, Cedex 4, France
Phone: +33-561558320 / *fax:* +33-561556701

M. Yamauchi <M.Yamauchi@irf.se>
Swedish Institute of Space Physics (IRF), Box 812, S-98128 Kiruna, Sweden

H. Rème <Henri.Reme@irap.omp.eu> (IRAP)

O. Marghitu <marghitu@gpsm.spacescience.ro>
Institute for Space Sciences (ISS), 409 Atomistilor Street, Magurele, Bucharest 077125, Romania

J. De Keyser <johandk@aeronomie.be >
Royal Belgian Institute for Space Aeronomy (BIRA-IASB), Ringlaan 3, B-1180 Brussels, Belgium

Scientific goal:

The ESCAPE mission will quantitatively estimate the amount (flux) of escape of the major atmospheric components (nitrogen N and oxygen O) as neutral and ionised species and at thermal and non-thermal forms, escaping from the Earth as a magnetised planet. The goal is to understand the importance of each escape mechanism and to infer the history of the Earth's atmosphere over a long (geological scale) time period. The spatial distribution and temporal variability of the flux of these elements and their isotopic composition will be investigated from the exobase/upper ionosphere (500 km altitude) up to the magnetosphere.

European SpaceCraft for the study of Atmospheric Particle Escape (ESCAPE)

Payload	* **Possible payload configuration: PI, PI institute, funding agency** - Cold ion and neutral mass spectrometer (M/ΔM > 1000): P. Wurz (PI), U. Bern, **Switzerland**. SSO - Light hot ions (M < 20, N/O separation, 10 eV/q – 30 keV/q): I. Dandouras (PI), IRAP, Toulouse, **France**. CNES - Heavy hot ions (M > 10, N/O separation, 10 eV/q – 30 keV/q): M. Wieser (PI), IRF, Kiruna, **Sweden**. SNSB - Energetic ions/electrons (H^+, He^+, O^{++}, N^+, O^+, N_2^+, 20 – 200 keV): L. Kistler (PI), Univ. New Hampshire, Durham, **USA**. NASA - Electrons (10 eV – 20 keV): A. Fazakerley (PI), UCL/MSSL, London, **UK**. UKSA - UV spectrometer (85 – 140 nm; optional: 391 nm and 428 nm): I. Yoshikawa (PI), Tokyo University, **Japan**. JAXA - Spacecraft potential (Langmuir probe): J. De Keyser (PI), BIRA-IASB, Brussels, **Belgium**. BELSPO - Magnetic field (5 nT accuracy): R. Nakamura (PI), IWF, Graz, **Austria**. ALR/FFG - Aurora/airglow camera (670 nm and 762 nm): T. Sakanoi, Tohoku U., **Japan**. JAXA - ENA imager (0.5 – 30 keV): A. Milillo (PI), INAF/IAPS, Rome, **Italy**. ASI - Waves (5 Hz – 20 kHz): B. Grison (PI), ASCR/IAP, Prague. **Czechia**. PRODEX J.-L. Pinçon (Co-PI), LPC2E, Orléans, **France**. CNES - Supplemental cold ion/neutral analyser (M/ΔM > 50): N. Paschalidis (PI), NASA/GSFC, **USA**. NASA * **Mandatory subsystems (by ESA)** - Spacecraft DPU, 5 m booms, Active spacecraft potential control
Orbit	- elliptic (500 km x 33000 km altitude with ~10 hr orbital period) - high-inclination (> 75°) to maximise geomagnetic conjugacy with EISCAT_3D - apogee will be either gradually increased or decreased


Geocoronal fine-structure cascade excitation constraints for ground-based observations

D. D. Gardner[1], E. J. Mierkiewicz[2], F. L. Roesler[1], S. M. Nossal[1]
[1]University of Wisconsin-Madison, [2]Embry-Riddle Aeronautical University - Daytona Beach, FL

PREFACE:

Night-time geocoronal Balmer-alpha (Hα) line profile shapes, obtained by high resolution Fabry Perot (FP), indicate a decrease in the cascade-contribution to the total geocoronal Hα observed intensity with viewing geometry (shadow altitude). Geocoronal Hα emission is comprised of 2 dominant fine structure (FS) transitions, and 7 FS cascade components (excited by solar Ly-β & Ly-$\gamma_>$, respectively).

THE PROBLEM:

Accurately accounting for cascade's redwing line-shape contribution is critical to interpreting individual line-shape observations for residual exospheric dynamic signatures. Poor cascade (or Galactic background) model fits can mask sought after dynamics, leading to misinterpretation of the geocoronal Hα line profile and erroneously high effective exospheric temperatures retrieved from the data-model fits.

COULD SCATTER IN FIG.1 BE AN SNR PROBLEM?

To test this hypothesis, we co-added the Hα spectra by consistent look-direction to increase the signal to noise ratio (SNR). This required corrections for instrumental drifts, Doppler-shifts (shown below), and spectral refitting using WHAM derived Galactic Hα background parameters, as well as our 7-component geocoronal FS cascade model.

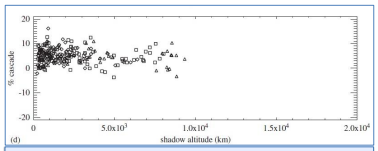

Figure 1:
Cascade contribution vs shadow altitude, as determined from individual FP geocoronal Hα line profile observations [Mierkiewicz at al., 2006]. Only observations towards regions of low galactic Hα background are plotted.

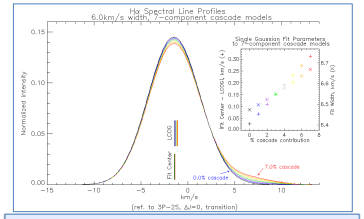

Figure 2:
Solar-illuminated geocoronal Hα profile models, illustrating varying cascade contribution at a constant temperature (6km/s, ~850 K a typical 3000 km shadow altitude).
Inset: systematic errors introduced to temperature and line center determination when cascade is ignored and fit with a single gaussion profile.

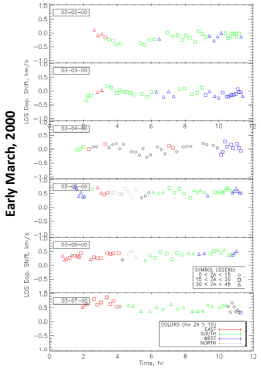

LOS Doppler-shifts in the Geocorona

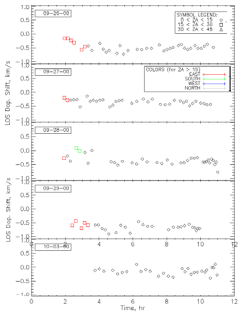

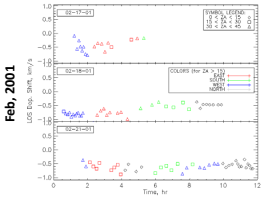

Figure 3:
Geocoronal Hα line profile LOS Doppler-shifts, observed by Fabry Perot from Pine Bluff, WI, plotted as a function of local observing hour past 6pm for 14 selected nights. All observations have been corrected for instrumental pressure shifts and residual temperature drifts. The absolute ordinate scale, [-1,+1] km/s, is tied to interspersed Thorium Argon lamp (6564 A) observations throughout each night.
Each 5-10 minute observation was tracked to regions with low (< 2 R) galactic Hα back-ground intensity. Night to night variations are on the order of 500 m/s. Dawn-dusk variations each night are on the order of 200 m/s, in line with exospheric H-model estimations (personal communication, J. Bishop).
Fall and winter observations show a significant average blue-ward bias when compared to the spring observations. This limited data set appears to corroborate seasonal exospheric temperature variations first reported by Mierkiewicz at al. (2012), pending further investigation here.

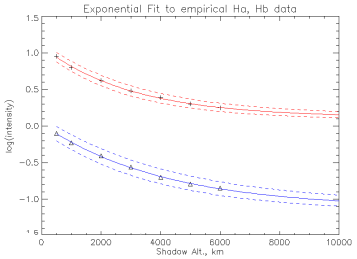

Figure 4:
WHAM observations of Hα & Hβ intensity, log(R) vs shadow altitude, (km). Overplotted are the (solid) exponential fits and (dashed) 1-σ parameter-error bands

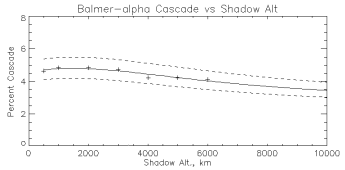

Figure 5:
Hβ/Hα derived cascade function (see text), and associated 1-σ parameter-error bands. Over plotted (plus symbols) are the unique values from the seven intensity ratios in Fig. 4 used for determination.

A UNIQUE SOLUTION:

Direct determination of Hα cascade with coincident Hα and Hβ measurements. Based on atomic physics, Roesler et al. (2014) theoretically demonstrated the total cascade in geocoronal Hα emission to be 0.52 ± 0.03 times geocoronal Hβ intensity. Hβ/Hα intensity ratios from the Wisconsin Hα Mapper FP (Fig. 4) were used to show a significantly narrowed range of uncertainty in the Hα cascade could be achieved for shadow altitudes lower than 6000 km.

Assuming a simple exponential decrease of log(intensity) with shadow altitude, we can extend a cascade parameterization out to 10,000 km shadow altitude. This empirically derived cascade function is consistent with previous cascade results determined directly from FP Hα line profile measurements. Further, it predicts a Hα cascade peak near 2000 km shadow altitudes, and convergence to a constant at higher shadow altitudes.

CONCLUSIONS:

Co-addition of Doppler-shift corrected geocoronal Hα line profiles and subsequent re-fitting to increase SNR does somewhat narrow cascade data scatter (shown in the Fig. 1), and the predicted cascade peak near 2000 km shadow altitude is also suggested (Fig. 6). Obviously, however, remaining data scatter and present lack of data to higher shadow altitudes precludes definitive data/cascade-parameterization comparison at this point.

In the absence of coincident Hβ & Hα intensity measurements, we anticipate a cascade function parameterization based on Roesler et al. (2014) and as shown here, to be useful in constraining cascade data fitting of future geocoronal Hα line profile observations. Cascade contributions to the geocoronal Hα line must be accounted for before conclusions of any residual redwing exospheric dynamics can be made, and to retrieve accurate exospheric temperatures.

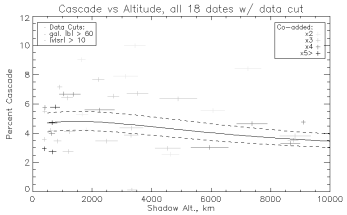

Figure 6:
(plus symbols) Cascade contribution, as determined from co-added and refit FP geocoronal Hα line profile observations (shown in Fig. 1). Darker colors indicate higher SNR by co-addition. Width indicates range of shadow altitudes co-added. Overplotted is the Fig. 5 predicted cascade behavior (& error) as determined by WHAM Hα and Hβ observations (Fig. 4)

References: [1] Mierkiewicz et al (2006) "Geocoronal hydrogen studies using Fabry-perot interferometers, part 1" J. Atm. Sol.Ter.Phys. 68, 1520-1552. [2] Mierkiewicz et al (2012) "Observed seasonal variations in exospheric effective temperatures" J. Geophysical Res. Vol. 117, A06313. [3] Roesler, F.L., E.J. Mierkiewicz, S.M. Nossal (2014), The Geocoronal Hα Cascade Component determined from Geocoronal Hβ Intensity Measurements, J. Geophys. Res. Space Physics, 119, 6642-6647. [4] Bishop, J., J.W. Chamberlain (1987), Geocoronal structure: 3. Optically thin, Doppler-broadened line profiles, J. Geophys. Res., 92(A11), 12389.

Acknowledgments: The authors are grateful for the NSF support of this work through awards AGS1352311 and AGS 1347687.

LOS Doppler-shifts in the Geocorona

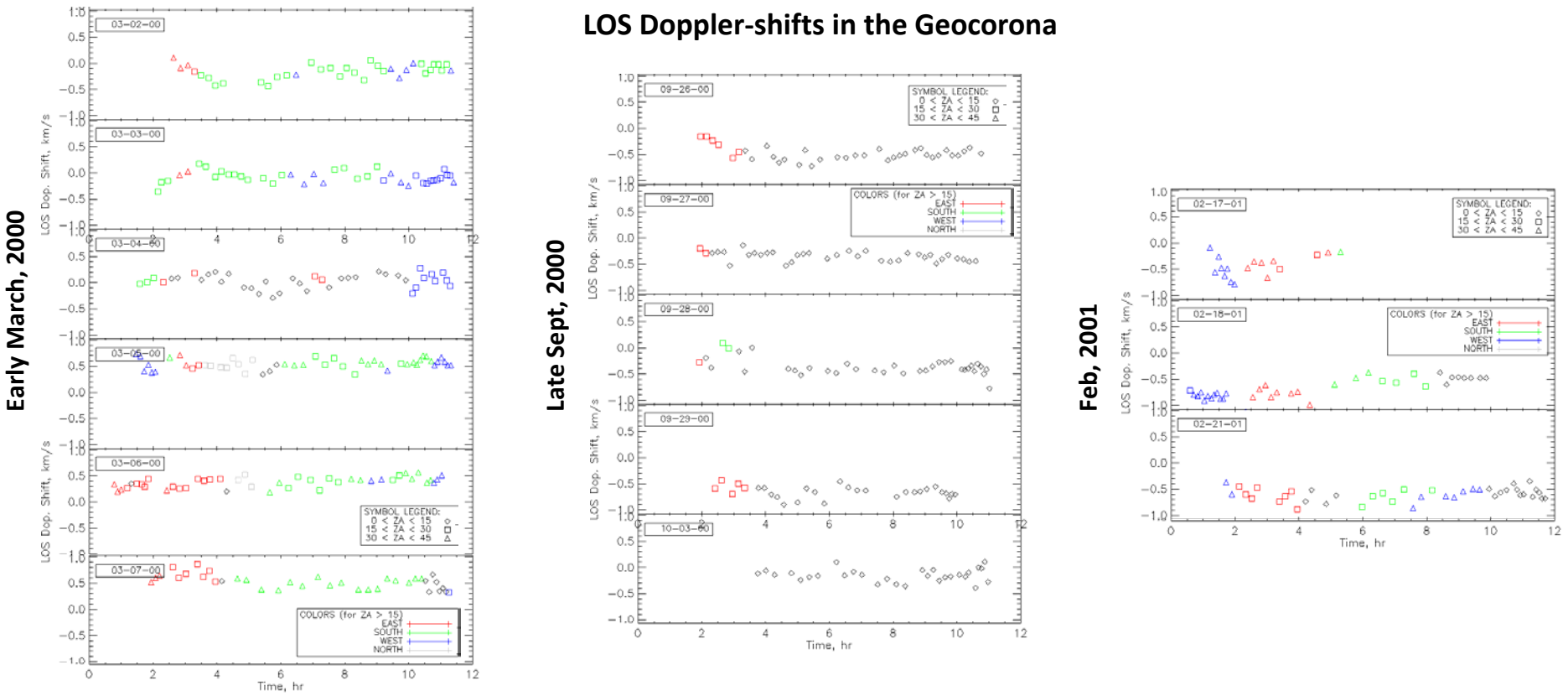

Figure 3:

Geocoronal Hα line profile LOS Doppler-shifts, observed by Fabry Perot from Pine Bluff, WI, plotted as a function of local observing hour past 6pm for 14 selected nights. All observations have been corrected for instrumental pressure shifts and residual temperature drifts. The absolute ordinate scale, [-1,+1] km/s, is tied to interspersed Thorium Argon lamp (6564 A) observations throughout each night.

Each 5-10 minute observation was tracked to regions with low (< 2 R) galactic Hα back-ground intensity. Night to night variations are on the order of 500 m/s. Dawn-dusk variations each night are on the order of 200 m/s, in line with exospheric H-model estimations (personal communication, J. Bishop).

Fall and winter observations show a significant average blue-ward bias when compared to the spring observations. This limited data set appears to corroborate seasonal exospheric temperature variations first reported by Mierkiewicz at al. (2012), pending further investigation here.

The small number of determinations of atomic hydrogen density profiles and fluxes has hindered the study of upper atmospheric atomic hydrogen distributions, limiting the compilation of empirical [H](z) and ϕ(H) models relevant to the testing of MLT photochemical models and impacting the prediction of lower exospheric densities needed for realistic modeling of geocoronal hydrogen density and ballistic flux distributions (Bishop, 2001).

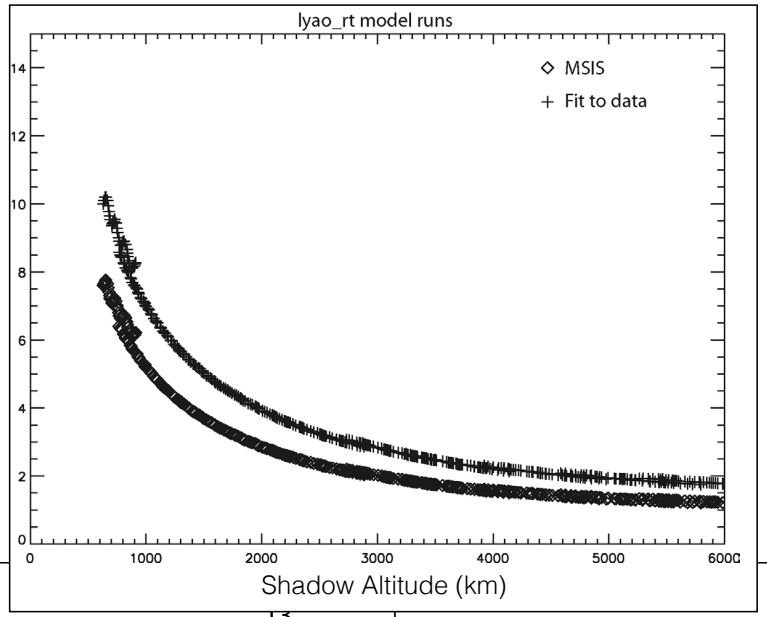

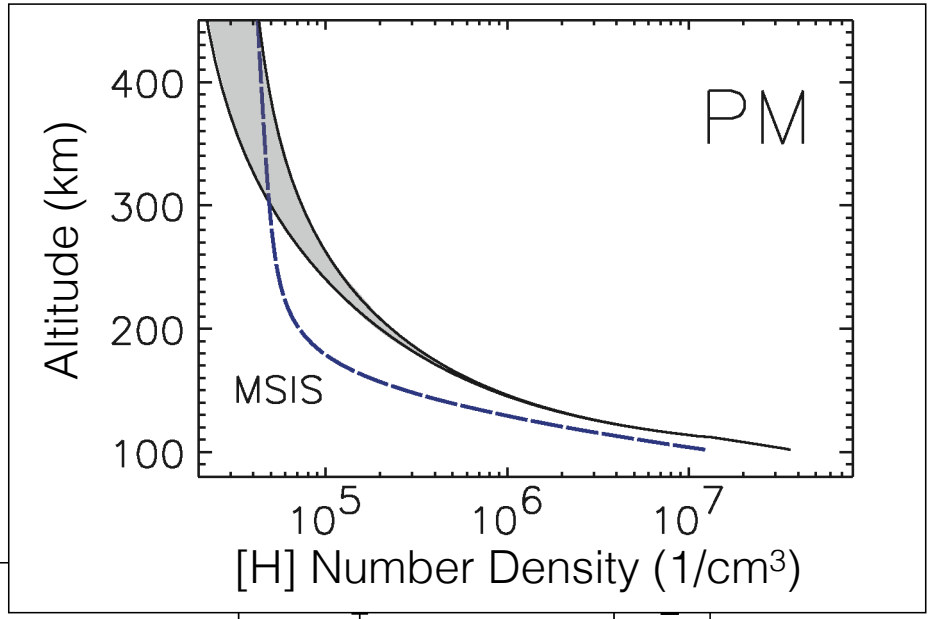

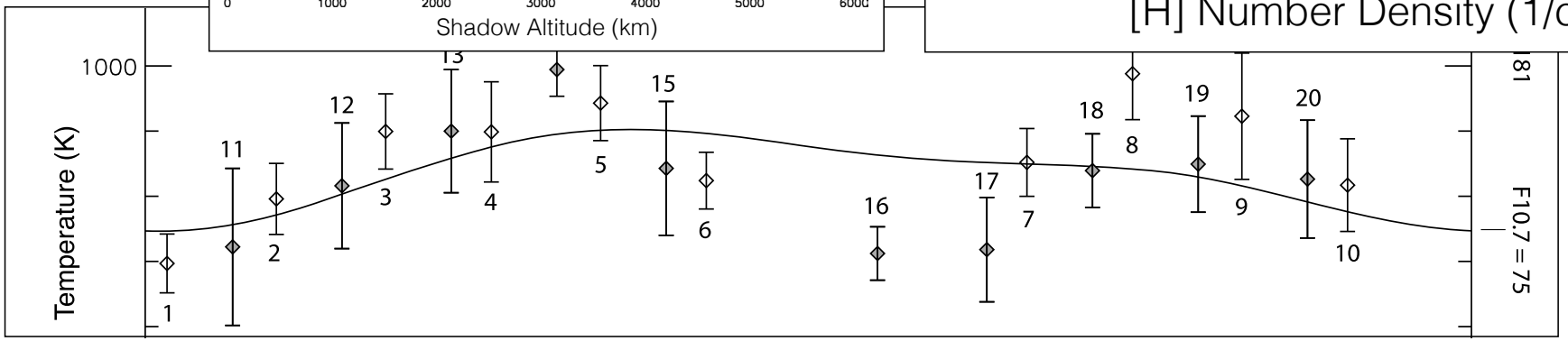

end